Electrical Supporting Information (ESI) for

Thermally activated delayed fluorescence with circularly polarized luminescence characteristics

Takuro Imagawa[1], Shuzo Hirata[2*], Kenro Totani[1],

Toshiyuki Watanabe[1] and Martin Vacha[2]

1. Department of Organic and Polymer Materials Chemistry, Tokyo University of Agriculture and Technology, 2-24-16 Naka, Koganei, Tokyo 184-8588, Japan
2. Department of Organic and Polymeric Materials, Tokyo Institute of Technology, 2-12-1, Ookayama, Meguro, Tokyo 152-8552, Japan

*Corresponding author.
E-mail: hirata.s.af@m.titech.ac.jp

This PDF file includes:

1. Explanation of an Advantage in Using an Emitter with Circularly Polarized Luminescence for Flat Panel Displays (Figure S1)

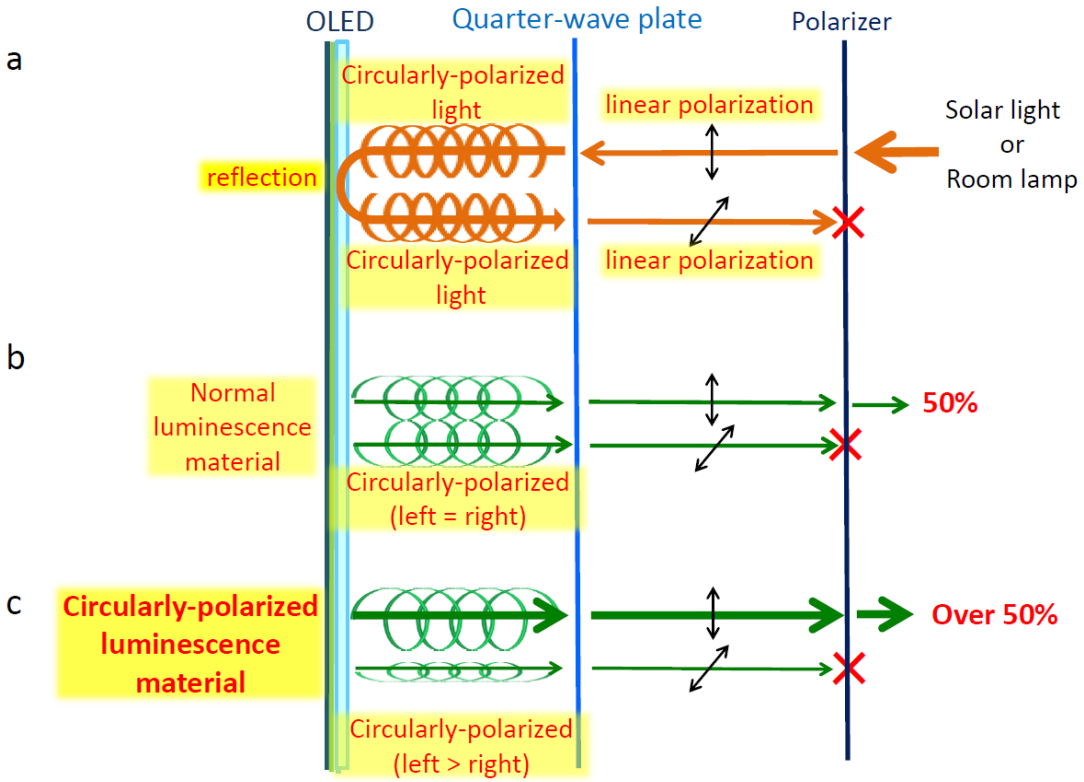

Figure S1 Illustrated explanation of the anti-reflection technique using a quarter-wave film and a polarizer on OLED display. (a) Half of the ambient external light, such as solar and room light, passes through the polarizer and it is reflected by the metal anode of the OLED. The reflected light is perfectly absorbed by the polarizer. (b) The left-handed electroluminescence from conventional TADF emitters in the OLED passes through the polarizer while the right-handed electroluminescence is absorbed by the polarizer. (c) OLED using TADF emitters with right-handed CPL characteristics mainly generates right-handed electroluminescence, which passes through the polarizer.

2. Synthesis and Characterization (Figures S2 and S3)

^{1}H and ^{13}C NMR spectra were recorded with a JNM-ECX400 spectrometer (JEOL Ltd., Japan) operating at 400 MHz for ^{1}H and 100 MHz for ^{13}C NMR experiments. Mass spectra were collected on a JMS-700D spectrometer (JEOL Ltd.) by means of fast atom bombardment.

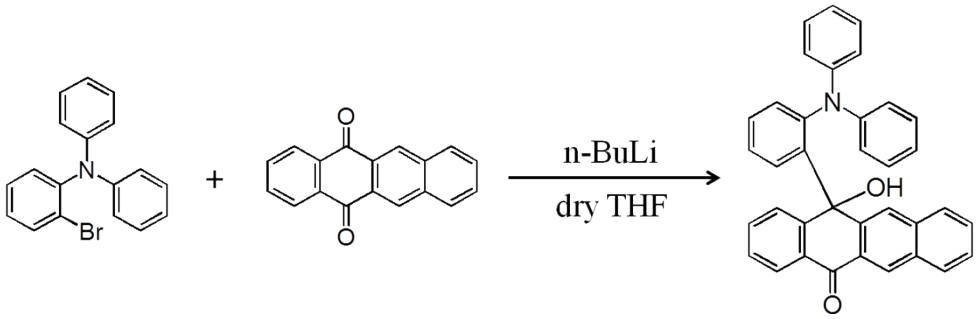

A solution of 2-bromotriphenylamine (7.75 mmol) in dry tetrahydrofuran (THF) (60 mL) was stirred at −78 °C under nitrogen for 30 min. After the slow addition of the 1.6 M n-BuLi hexane solution (4.8 mL) to the solution, the solution was stirred under nitrogen at −78 °C for 1.5 h. Next, 5,12-naphthacenequinone (7.07 mmol) was added to the solution and the solution was stirred at 0 °C for 24 h. The solution was evaporated to remove THF, and chloroform (100 mL) was added. The organic phase was washed with ice H_2O (50 mL×3), dried over sodium sulfate (Na_2SO_4), and then filtered. Evaporation of the filtrate gave the crude product, which was purified by column chromatography (silica gel; eluent = chloroform) to give racemic 12-(2-(diphenylamino)phenyl)-12-hydroxynaphthacen-5(12*H*)-one (DPHN) as a yellow powder (1.69 g, 3.36 mmol, 47.5%). ^{1}H NMR (400MHz, dimethyl sulfoxide (DMSO)-d_6) : δ (ppm) 5.84 (dd, *J*=6.0 Hz, *J*=8.2 Hz, 4H), 6.18 (t, *J*=7.1 Hz, 1H), 6.29 (t, *J*=7.3 Hz, 2H), 6.69 (m, 4H), 6.91 (s 1H), 7.29 (t, *J*=7.3, 1H), 7.38 (t, *J*=7.8, 2H), 7.45 (t, *J*=7.8, 1H), 7.52 (q, *J*=7.6, 2H), 7.60 (t, *J*=7.3, 1H), 7.69 (s, 1H), 7.80 (d, *J*=8.2, 1H), 7.86 (d, *J*=7.8, 1H), 7.94 (d, *J*=8.3 1H), 8.38 (s 1H), 8.77 (d, *J*=8.3 1H); ^{13}C NMR (100 MHz, DMSO-d_6): δ (ppm); 183.35, 148.40, 147.22, 147.12, 145.08, 144.20, 142.53, 135.59, 133.82, 133.38, 131.83, 130.34, 129.92, 129.87, 129.82, 128.97, 128.66, 128.53, 128.13, 128.08, 127.76, 127.55, 127.41, 126.75, 122.03, 121.74, 121.38, 70.54; HRMS-FAB (*m*/*z*): $[M]^+$ calcd. for $C_{36}H_{25}NO_2$, 503.19; found, 503.19. The results of the ^{1}H NMR and ^{13}C NMR are shown in Fig. S1a and b, respectively. The result of the mass analysis is shown in Fig. S2a. The enantiomers of DPHN were separated using a LC-2000Plus Series System (Jasco,

Japan) attached with a Chiralpak ID (Daicel, Japan) using an eluent = 20% ethylacetate/hexane as shown in Fig. S2b.

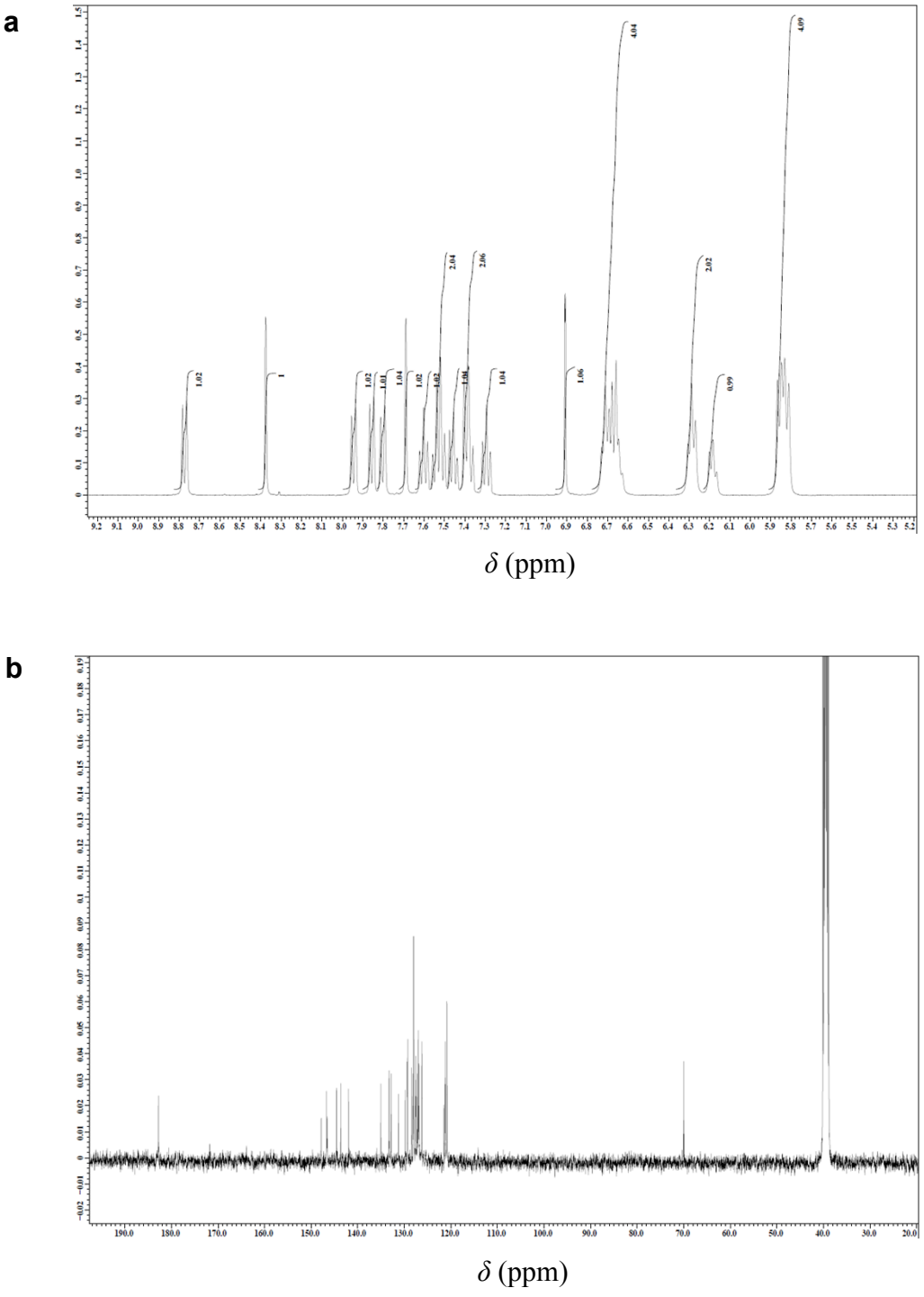

Figure S2 1H-NMR(a) and 13C-NMR(b) spectra of DPHN in DMSO-d_6.

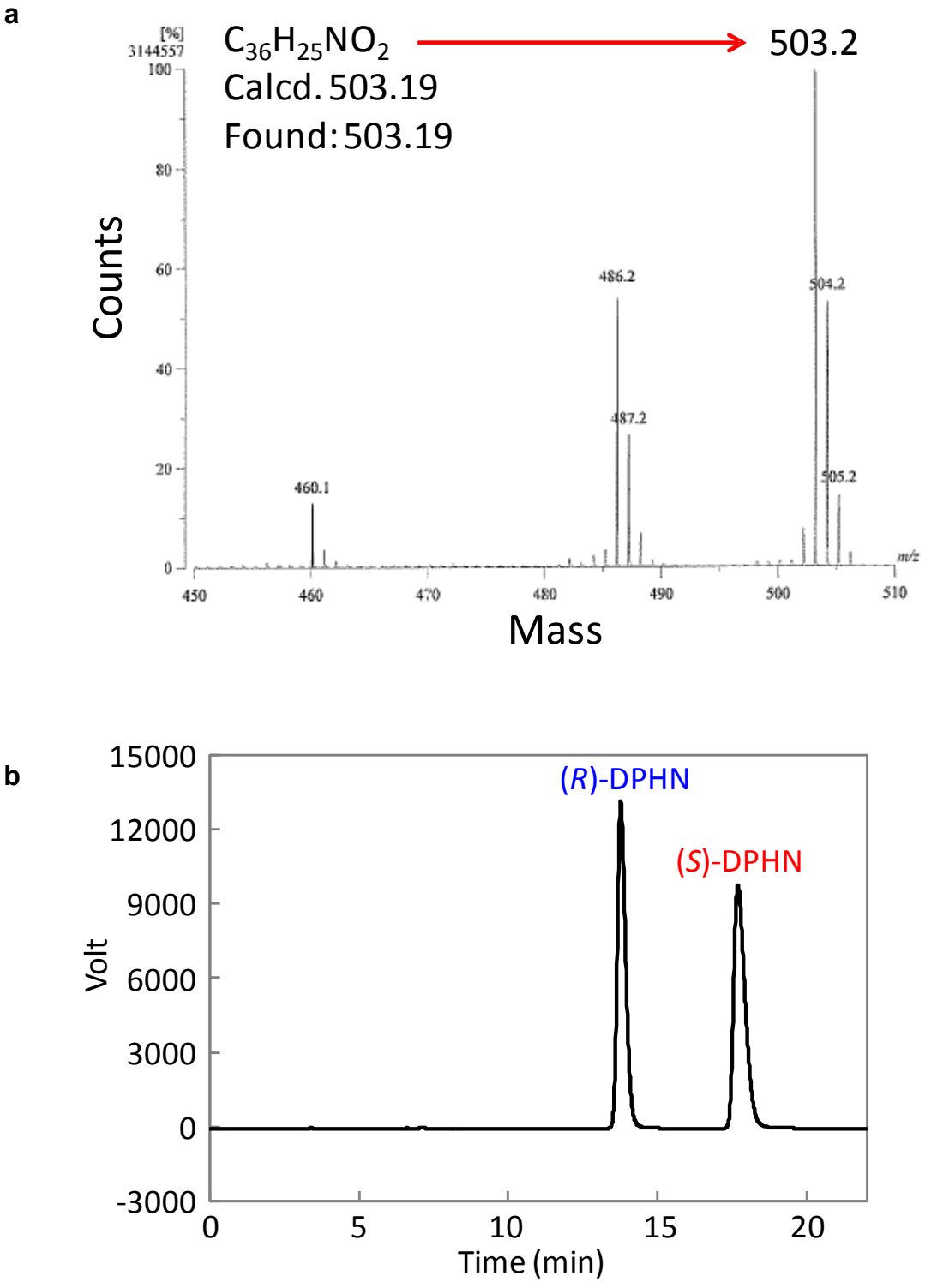

Figure S3 (a) HRMS-FAB spectra of DPHN. (b) Optical resolution of DPHN in a high-pressure liquid chromatography measurement.

3. Photophysical Characteristics of an Emitter with Circularly Polarized Luminescence (Figure S4)

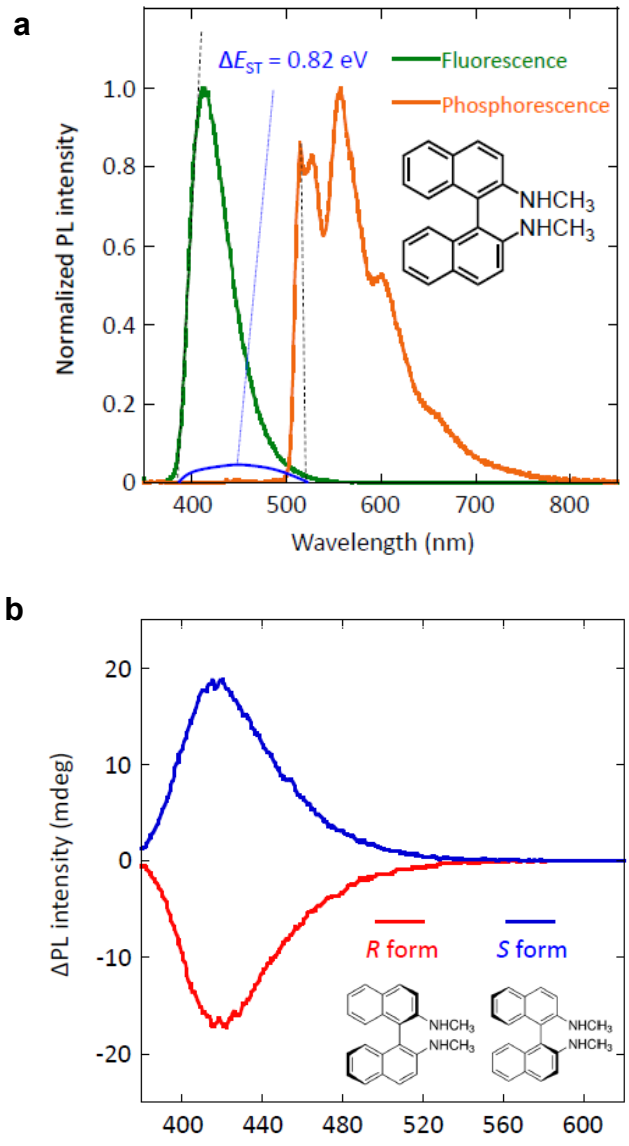

Figure S4 Spectral characteristics of N,N'-dimethyl-1,1'-binaphthyldiamine in toluene. (a) Fluorescence spectrum at room temperature (blue) and phosphorescence spectrum at 77K (orange). Inset shows chemical structure of N,N'-dimethyl-1,1'-binaphthyldiamine. Dotted lines represent supporting lines to determine S_1 and T_1 energy. (b) Circularly polarized luminescence (CPL) spectra of (*R*)-N,N'-dimethyl-1,1'-binaphthyldiamine (blue) and (*S*)-N,N'-dimethyl-1,1'-binaphthyldiamine (red). The dissymmetric factor of the CPL was $|1.2\times10^{-3}|$. The inset shows chemical structures of the (*R*) and (*S*) forms.

4. Determination of Oscillator Strength for Absorption and Fluorescence (Figure S5)

The oscillator strength for absorption (F) is typically expressed using the following equation,[14]

$$F = 4.32 \times 10^{-9} n^{-1} \int \varepsilon(\nu) d\nu , \quad \text{(S1)}$$

where n is the refractive index, ν is the wavenumber (in cm^{-1}), and $\varepsilon(\nu)$ is the molar absorption coefficient of the structure at the ground state (S_0) at ν (in 10^3 cm^2 mol^{-1}). Because the absorption spectrum of Fig. 2a contains multiple absorption bands, the absorption spectrum was deconvoluted using four Gaussian functions as shown in Fig. S5. The absorption with the lowest absorption wavenumber (red dotted line) corresponds to the first CT absorption band of DPHN. The values of $\int \varepsilon(\nu) d\nu$ in the CT absorption were used to determine F.

Next, the rate constant of fluorescence (k_f) is expressed as,[16]

$$k_f = 2.88 \times 10^{-9} n^2 \nu_{max}^{\ 2} \int \varepsilon'(\nu) d\nu , \quad \text{(S2)}$$

where ν_{max} is the wavenumber at the fluorescence peak and $\varepsilon'(\nu)$ is the molar absorption coefficient of the structure at the lowest singlet excited state (S_1) at ν (in 10^3 cm^2 mol^{-1}). The oscillator strength of fluorescence (F') is expressed as,

$$F' = 4.32 \times 10^{-9} n^{-1} \int \varepsilon'(\nu) d\nu . \quad \text{(S3)}$$

For the determination of F', the value of $\int\varepsilon'(v)dv$ was determined by substituting the fluorescence spectrum into equation (S2). Then, the value of F' was calculated using equation (S3).

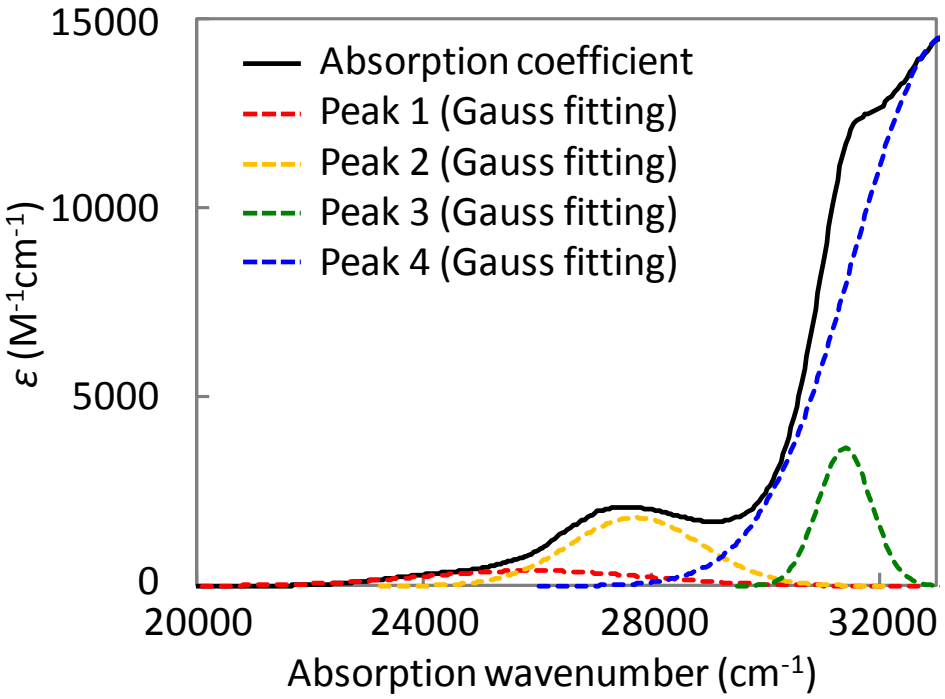

Figure S5 Determination of each absorption band by Gaussian fittings. The black line represents $\varepsilon(v)$ *vs*. v characteristics of DPHN. Red, orange, green, and blue dotted lines represent fitting curves when the black spectrum is expressed by a summation of the Gaussian curves.

5. Fluorescence Lifetime in Toluene Solution (Figure S6)

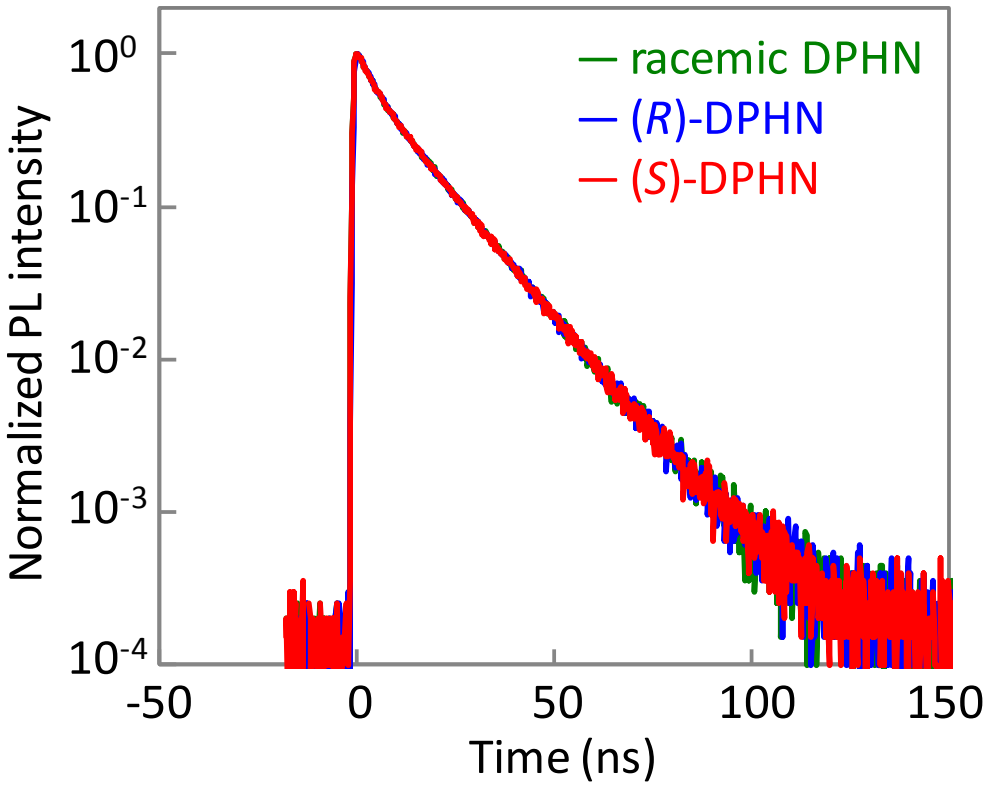

Figure S6 Emission decay characteristics of racemic DPHN, (*R*)-DPHN, and (*S*)-DPHN in toluene solution in air.

6. Details of Time-Dependent DFT Calculations (Figures S7-S10 and Tables S1-S3)

6.1 Contribution of a variety of conformations optimized at S_0 to CD peaks

Local minimum structures at S_0 were explored using Conflex (CONFLEX 7 Rev. 3). The results showed that (*R*)-DPHN has four kinds of local minimum conformations. Because the conformation determined by Conflex is still rough, the four conformations are again optimized at S_0 by using DFT (Gaussian09/B3LYP/6G31(d.p)), resulting in appearance of four optimized S_0 conformations (I)-(III) as shown in Fig. S7. Finally, the various parameters such as the relative absolute energy of conformation (*E*), the wavelength at first absorption band (λ), the oscillator strength for absorption (*F*), $\Delta\varepsilon$, and the angle between electronic transition dipole moment and magnetic transition dipole moment (θ) were calculated for conformations (I)-(III).

Table S1 presents various parameters of conformations (I)-(III). The existence ratio (*N*) of conformations (I), (II), and (III) was determined as 74, 17, and 9% based on Arrhenius distribution at room temperature using *E* of the conformations, respectively. Therefore, (*R*)-DPAN at S_0 mainly has conformation (I) at room temperature. Figure S8a; (ii) shows the relationship between *NF* and λ of (*R*)-DPHN, which corresponds to theoretical absorption spectrum of (*R*)-DPHN. The theoretical absorption spectrum (Fig. S8a (ii)) shows that (*R*)-DPHN has a large absorption peak at 363 nm caused by $S_0 \rightarrow S_2$ transition with π-π^* character. Conformation (I) has a main CT peak at 367 nm, which corresponds to $S_0 \rightarrow S_1$ transition. Minor conformations (II) and (III) have two small CT peaks at wavelength longer than 367 nm. The shape of the theoretical absorption spectrum of ((ii) of Fig. S8a) has similar tendency to that of experimentally observed absorption spectra ((i) of Fig. S8a). Figure S8b, (i) represents the relation between $N\Delta\varepsilon$

a

Conformation	Molecular orbitals relating transition at first absorption band: Before absorption	Molecular orbitals relating transition at first absorption band: After absorption	Control factor
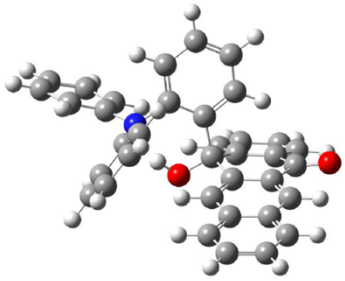	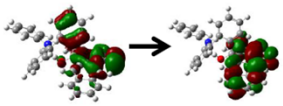		0.56592

b

Conformation	Molecular orbitals relating transition at first absorption band: Before absorption	Molecular orbitals relating transition at first absorption band: After absorption	Control factor
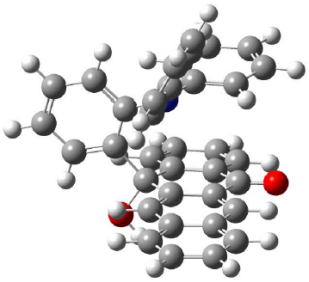	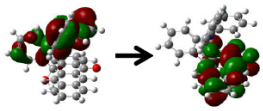		0.70506

c

Conformation	Molecular orbitals relating transition at first absorption band: Before absorption	Molecular orbitals relating transition at first absorption band: After absorption	Control factor
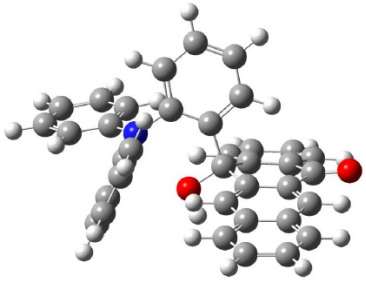	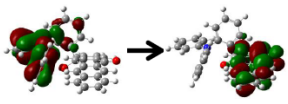		0.70649

Figure S7 Conformations (I)-(III) of (*R*)-DPHN optimized at S_0 and their molecular orbitals the transition relating first absorption band. (a) Conformation (I). (b) Conformation (II). (c) Conformation (III).

Table S1 Photophysical parameters at first absorption band of conformations (I)-(III) in (*R*)-DPHN.

Conformation	E^* (eV)	N (%)	λ (nm)	F ($\times 10^{-3}$)	$\Delta\varepsilon$ (M^{-1} cm^{-1})	NF ($\times 10^{-3}$)	$N\Delta\varepsilon$ (M^{-1} cm^{-1})	cosθ	θ (deg.)
(I)	0	74	367	2.1	-0.4176	1.56	-0.3107	-0.82	145
(II)	0.0373	17	488	3.6	0.0502	0.60	0.0084	0.53	58
(III)	0.0528	9	496	0.1	-0.0082	0.009	-0.0007	-0.59	126

*: Relative energy when absolute energy of conformation (I) is 0.

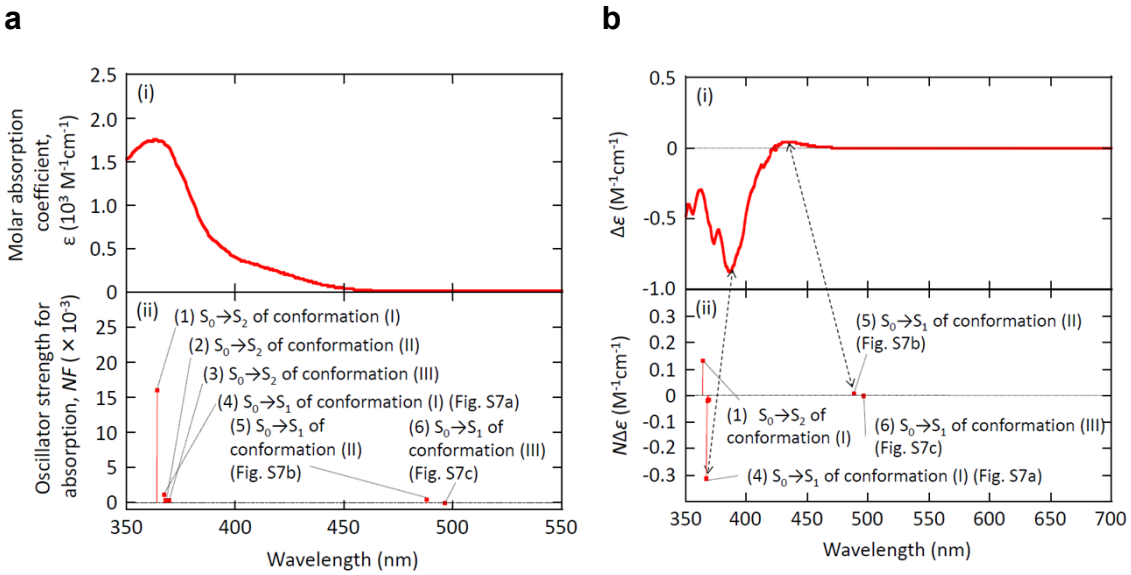

Figure S8 Absorption (a) and CD (b) spectra of (*R*)-DPHN. (i) Experimentally obtained spectra of (*R*)-DPHN in toluene. (ii) Calculated spectra by TD-DFT(Gaussian09/B3LYP/6G31(d.p)) using conformations (I)-(III).

and λ of (*R*)-DPHN, which corresponds to theoretical CD spectrum of (*R*)-DPHN. The theoretical CD spectra suggests that (*R*)-DPHN has a main negative CD peak at 367 nm, a small positive CD peak at 488 nm, and a very small negative peak at 496 nm shown in Fig. S8b, (ii) (We note that the very small negative CD peak at 496 nm does not appear because it may be hidden in the positive CD peak at 488 nm). As shown in Fig. S8b, the theoretical CD spectrum ((ii) of Fig. S8b) showed very similar tendency to experimentally observed one ((i) of Fig. S8b). Therefore, absorption showing negative CD peak at 386 nm is caused by the transition of conformation (I) shown in (a) of Fig. S7 and absorption showing positive CD peak at 430 nm is mainly caused by the transition of conformation (II) shown in (b) of Fig. S7.

The transitions shown in (a)-(c) of Fig. S7 contain CT character from HOMO in TPA unit to LUMO in UC unit. For conformations (I) and (III), the TPA and NC units are almost symmetric with respect to the chiral carbon in the S_0. In conformation (I), the value of cosθ is negative (Table S1), causing the negative CE for CD. On the other hand, the NC unit position substantially changes in the conformations (II) as the TPA get close to the NC position. In the conformations (II), the value of cosθ is positive, causing the positive CD. The negative CD intensity caused by $S_0 \rightarrow S_1$ transition of conformation (I) in Fig. S8b is large compared with that caused by $S_0 \rightarrow S_1$ transition of other two conformations because the values of N and $\Delta\varepsilon$ of conformation (I) is larger than those of conformations (II) and (III) (Table S1). The small values of the CD peaks caused by $S_0 \rightarrow S_1$ transition of conformations (II) and (III) in Fig. S8b are caused by the small existence ratio as well as the small $\Delta\varepsilon$ in the conformations.

6.1 A variety of conformations optimized at S_1

Conformation (I)-(III) was used as starting conformation to estimate local minimum S_1 structures by TD-DFT calculation (Gaussian09/B3LYP/6G-31(d.p)), resulting in appearance of two conformations (conformation (IV) and (V)) of (*R*)-DPHN at S_1, as shown in Fig. S9. Table S2 presents photophysical parameters of conformations (IV) and (V). In Table S2, *F*' and *λ*' represents the oscillator strength for fluorescence and fluorescence energy, respectively. The existence ratio (*N*) of conformations (VI) and (V) was determined as 66 and 34% based on Arrhenius distribution at room temperature

a

Conformation	Molecular orbitals relating fluorescence		Control factor
	Before fluorescence	After fluorescence	
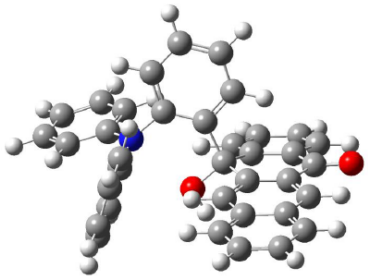	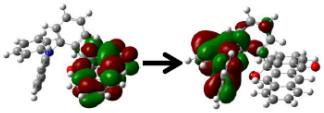		0.70657

b

Conformation	Molecular orbitals relating fluorescence		Control factor
	Before fluorescence	After fluorescence	
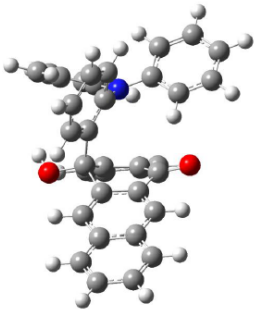	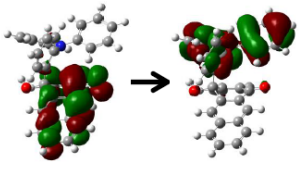		0.70483

Figure S9 Conformations (IV) and (V) of (*R*)-DPHN optimized at S_1 and their molecular orbitals relating fluorescence. (a) Conformation (IV). (b) Conformation (V).

Table S2 Photophysical parameters at the lowest singlet excited state of the conformations (IV) and (V) in (*R*)-DPHN.

Conformation	E^* (eV)	N (%)	λ' (eV)	F' ($\times 10^{-3}$)	$\Delta\varepsilon$ (M^{-1} cm^{-1})	NF' ($\times 10^{-3}$)	$N\Delta\varepsilon$ (M^{-1} cm^{-1})	cosθ	θ (deg.)
(IV)	0	66	2.35	<0.1	-0.0031	<0.03	-0.0021	-0.0008	117
(V)	0.0164	34	1.84	1.5	0.1365	0.51	0.0467	0.70	46

*: Relative energy when absolute energy of conformation (IV) is 0.

, respectively. As shown in the values of $N\Delta\varepsilon$ in Table S2, conformation (VI) has negative CPL but it is significantly small because of small cosθ. In addition, because conformation (VI) has significant small NF" caused by small F", it is considered that fluorescence quantum yield of conformation (IV) will be nearly 0. On the other hand, conformation (V) has large F" compared with conformation (IV), allowing generation of fluorescence. Because $\Delta\varepsilon$ of conformation (V) is positive and it is much larger compared with conformation (VI), positive CPL was observed from (*R*)-DPHN.

6.2 A variety of conformations optimized at T_1

Conformation (I)-(III) were used as starting conformations to estimate local minimum T_1 structures by TD-DFT calculation (Gaussian09/B3LYP/6G-31(d.p)), resulting in the appearance of three conformations (conformation (VI)-(VIII)) of (*R*)-DPHN at T_1, as shown in Fig. S10. Table S3 presents photophysical parameters of conformation (VI)-(VIII). The ratio (N) of conformations (VI), (VII), and (VIII) was determined as 76%, 16%, and 8%, respectively, based on the Arrhenius distribution at room temperature using E of the conformations. The most populated conformation (VIII) shows π-π* characteristics.

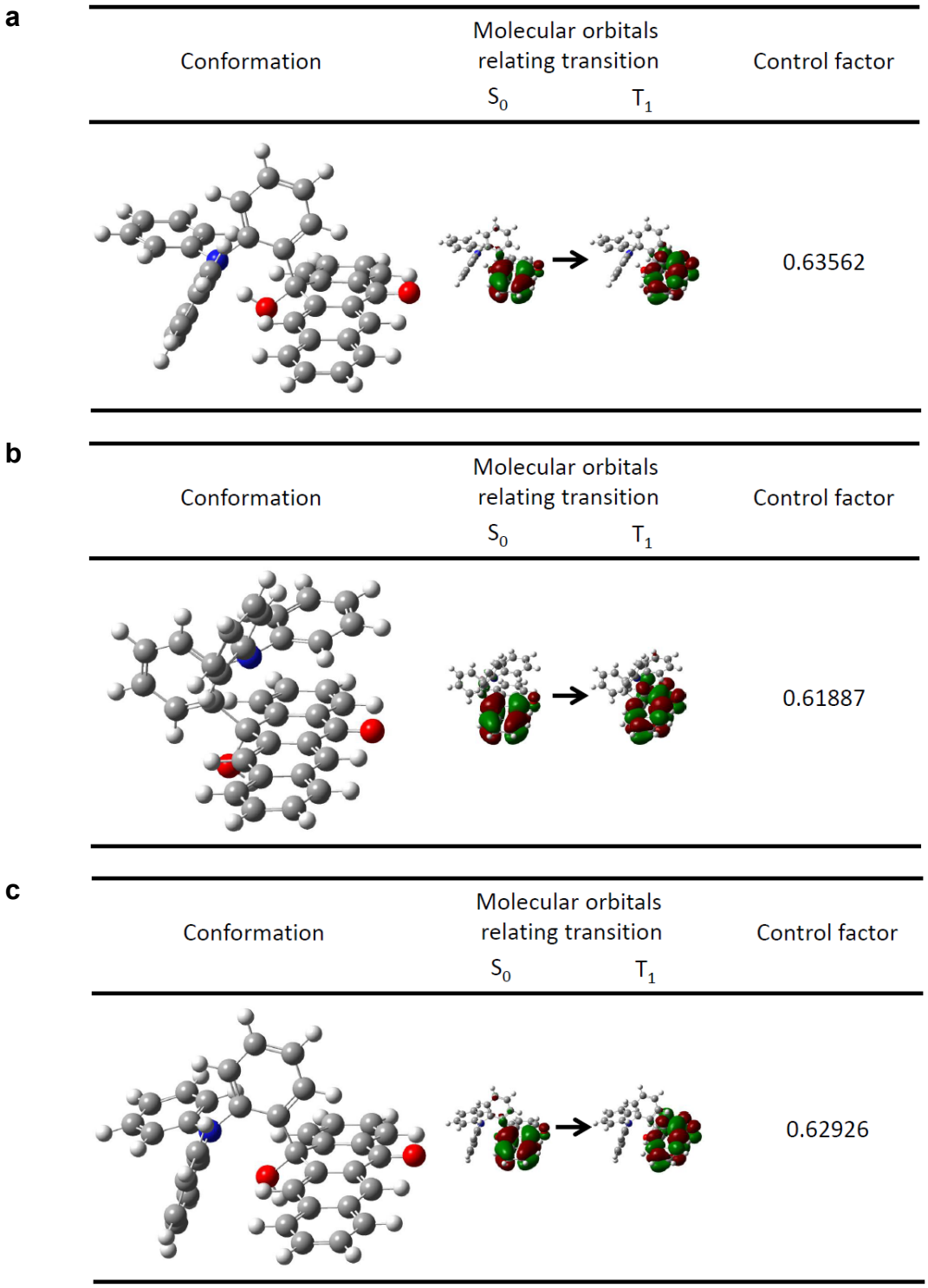

Figure S10 Conformations (VI)-(VIII) of (*R*)-DPHN optimized at T_1 and their molecular orbitals involved in the transition to T_1. (a) Conformation (VI). (b) Conformation (VII). (c) Conformation (VIII).

Table S3 Photophysical parameters of conformations (VI)-(VIII) of (*R*)-DPHN.

Conformation	E^* (eV)	N (%)	λ (eV)	cosθ	θ (deg.)
(VI)	0	76	1.77	0.65	99
(VII)	0.0381	16	1.75	0.46	126
(VIII)	0.0574	8	1.77	0	90

*: Relative energy when absolute energy of conformation (VI) is 0.

7. Details of experimental procedures used to measure photophysical characteristics (Figure S11)

Ultraviolet (UV)-visible absorption and CD spectra of 3.3×10^{-4} M DPHN in toluene were measured using a UV-visible absorption spectrometer (V-560, Jasco, Japan) and a CD dispersion meter (J-720, Jasco). Solutions of (*R*)-DPHN and (*S*)-DPHN in toluene (2.5×10^{-3} M) were used to measure CD spectra at 400–500 nm. Emission and CPL spectra of (*R*)-DPHN, (*S*)-DPHN, and racemic DPHN in toluene (8.8×10^{-5} M) were measured using a multichannel analyzer (PMA-12, Hamamatsu, Japan) and a spectrofluoropolarimeter (CPL-200, Jasco), respectively. For photoluminescence and CPL spectra, light of 360 nm was used as an excitation source.

DPHN-doped mCP films with various contents of DPHN were prepared on quartz substrates by spin casting from chloroform solutions. Figure S11 shows the relationship between photoluminescence quantum yield (Φ_{PL}) and the concentration of DPHN for the DPHN-doped mCP films under excitation light of 340 nm. The film with a DPHN concentration of 9 wt% showed the largest Φ_{PL}. Therefore, we characterized the photophysical characteristics of the 9 wt% DPHN-doped mCP film.

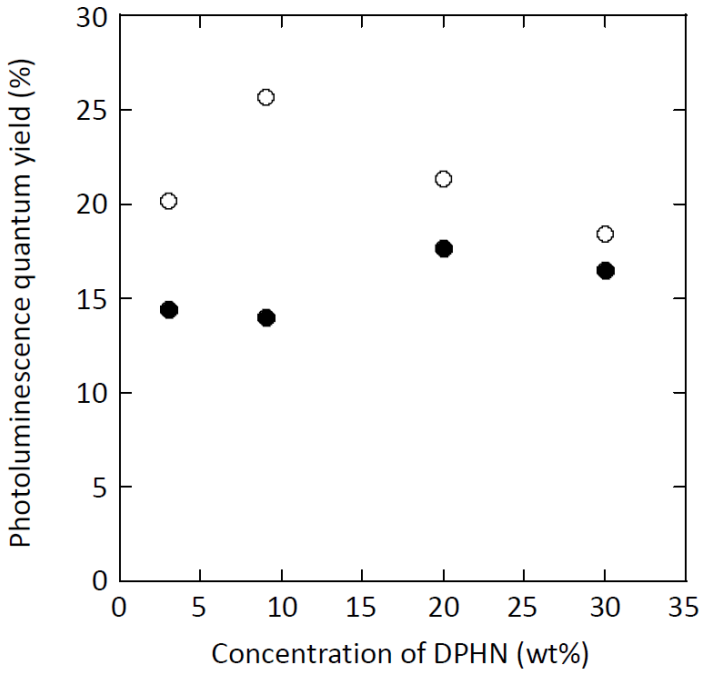

Figure S11 Relationship between photoluminescence quantum yield under excitation at 340 nm and concentration of DPHN for DPHN-doped mCP films.

8. Temperature Dependence of the Emission Lifetime (Figure S12)

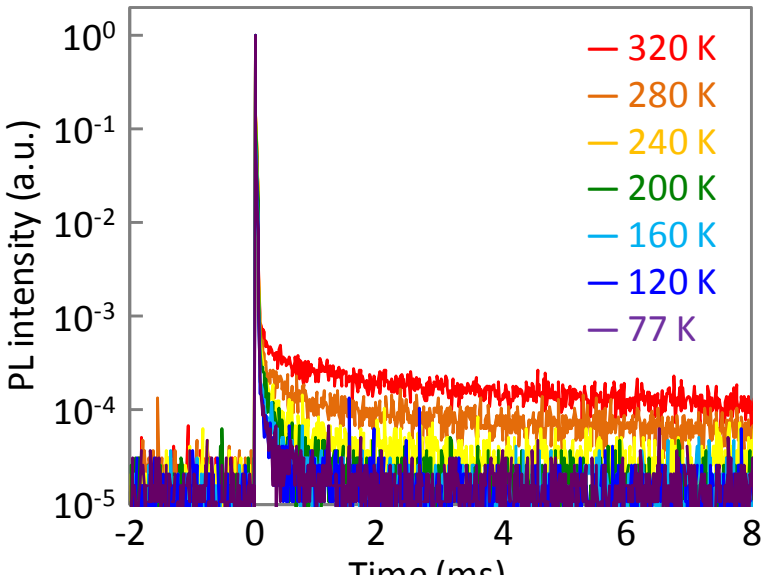

Figure S12 Temperature dependence of emission decay characteristics of 9 wt% racemic DPHN doped mCP film under vacuum conditions. Light at 340 nm was used as an excitation pulse.